LIMNOLOGY and OCEANOGRAPHY: METHODS

ASLO

Limnol. Oceanogr.: Methods 2022

doi: 10.1002/lom3.10530

Novel device to collect deep-sea porewater in situ: A focus on benthic carbonate chemistry

Jaclyn E. P. Cetiner,[1]* **William M. Berelson**,[1] **Nick E. Rollins**,[1] **Holly A. Barnhart**,[2] **Xuewu Liu**,[3] **Sijia Dong**,[2] **Robert H. Byrne**,[3] **Jess F. Adkins**[2]

[1]University of Southern California, Los Angeles, California
[2]California Institute of Technology, Pasadena, California
[3]University of South Florida, St. Petersburg, Florida

Abstract

We have designed, built, tested, and deployed a novel device to extract porewater from deep-sea sediments in situ, constructed to work with a standard multicorer. Despite the importance of porewater measurements for numerous applications, many sampling artifacts can bias data and interpretation during traditional porewater processing from shipboard-processed cores. A well-documented artifact occurs in deep-sea porewater when carbonate precipitates during core recovery as a function of temperature and pressure changes, while porewater is in contact with sediment grains before filtration, thereby lowering porewater alkalinity and dissolved inorganic carbon (DIC). Here, we present a novel device built to obviate these sampling artifacts by filtering porewater in situ on the seafloor, with a focus near the sediment–water interface on cm-scale resolution, to obtain accurate porewater profiles. We document 1–10% alkalinity loss in shipboard-processed sediment cores compared to porewater filtered in situ, at depths of 1600–3200 m. We also show that alkalinity loss is a function of both weight % sedimentary $CaCO_3$ and water column depth. The average ratio of alkalinity loss to DIC loss in shipboard-processed sediment cores relative to in situ porewater is 2.2, consistent with the signal expected from carbonate precipitation. In addition to collecting porewater for defining natural profiles, we also conducted the first in situ dissolution experiments within the sediment column using isotopically labeled calcite. We present evidence of successful deployments of this device on and adjacent to the Cocos Ridge in the Eastern Equatorial Pacific across a range of depths and calcite saturation states.

Accurate porewater measurements are necessary for myriad oceanographic and geochemical applications: modeling fluxes of nutrients and major ions (Berelson et al. 1987; Martin et al. 1991; Sun et al. 2016; Hou et al. 2019); sediment diagenesis (Froelich et al. 1979; Sayles 1979; Emerson et al. 1980; Jahnke et al. 1994); paleoclimate reconstructions (Schrag et al. 1996; Higgins and Schrag 2012; Blättler et al. 2019); constraining model projections of the oceans' response to climate perturbations (Archer et al. 1998; Sulpis et al. 2018), among many others. Of particular interest to our group is an effort to understand benthic carbonate diagenesis, dissolution fluxes (Jahnke et al. 1997; Martin and Sayles 2006; Berelson et al. 2007), and address the sediment vs. water-side control of alkalinity fluxes from carbonate dissolution, that is, identifying to what extent dissolution occurs at or below the sediment–water interface (SWI) (Boudreau 2013; Sulpis et al. 2017).

The invasion of anthropogenic CO_2 leads to acidified surface water eventually making its way to the deep ocean. There is evidence in the geologic record that Earth has naturally corrected for high concentrations of CO_2 and returned to a state of equilibrium (Foster and Rohling 2013) via reactions on the deep-sea floor that neutralize acid, but this process is thought to occur on the order of 10,000 yr (Archer et al. 2009). Critical outstanding questions remain regarding precisely how fast dissolved CO_2 will react with $CaCO_3$, how this reaction occurs as a function of seawater saturation state, and where in the sediment column dissolution occurs. However, typical porewater processing, for example, collecting a

*Correspondence: jepittma@usc.edu

Author Contribution Statement: J.E.P.C., W.M.B., N.E.R., and J.F.A. conceptualized the study. J.E.P.C., N.E.R., H.A.B., X.L., and S.D. collected data. J.E.P.C., W.M.B., N.E.R., H.A.B., S.D., and J.F.A. analyzed data. X.L. and R.H.B. provided new methodology for carbonate measurements. W.M.B. and J.F.A. acquired funding. J.E.P.C. wrote the original manuscript draft. All authors contributed to reviewing and editing manuscript draft.

sediment core and filtering, squeezing, or centrifuging sediment to isolate porewater, can result in sampling artifacts associated with pressure and temperature changes that alter the concentrations of porewater species. Much work remains to be done studying carbonate dissolution at and below the SWI, in large part because of the challenges associated with obtaining artifact-free carbonate chemistry porewater profiles.

One outstanding question regarding benthic carbonate dissolution studies relates to the role of organic carbon respiration and carbonic acid formation as a driver of dissolution (Emerson and Bender 1981). Whether this process occurs mainly at the SWI or deeper within the sediment column is difficult to assess without artifact-free, high-resolution profiles. Although carbonate dissolution kinetics have recently been well studied in the lab (Subhas et al. 2015; Dong et al. 2018; Naviaux et al. 2019*a*) and water column (Dong et al. 2019; Naviaux et al. 2019*b*, summarized by Adkins et al. 2021), accurate porewater profiles and in situ carbonate dissolution experiments will also help complete our understanding of carbonate dissolution kinetics. Because of the importance of studying benthic carbonate chemistry and because of the inherent difficulties of obtaining artifact-free porewater, we developed a novel instrument to collect filtered porewater in situ from deep-sea sediments and to perform the first in situ benthic dissolution rate experiments.

Conducting measurements in situ has long been recognized as a way to obviate pressure and temperature artifacts associated with sample return to the surface. The work with in situ pH, pCO_2, and O_2 microelectrodes (Reimers et al. 1992; Glud et al. 1994; Hales et al. 1994) provided breakthrough capabilities, yet they could not probe more than a few cm into the sediment column, potentially not reaching below the depth of oxygen penetration which is necessary to study the suite of diagenetic reactions occurring in shallow sediments. The WHIMP harpoon sampler was developed to compare porewater collected in situ to that collected through traditional methods of porewater extraction, that is, core recovery and squeezing (Sayles et al. 1973). Sayles et al. (1973) found that Ca and Mg were depleted, and K enriched in cores processed onboard a ship compared to in situ collection. This harpoon system was the basis for several foundational in situ porewater studies (Sayles et al. 1976; Murray et al. 1980; Sayles 1981), in which ex situ depletions and enrichments were further documented and attributed to the pressure effect, that is, the pressure decrease from seafloor to surface drives changes in saturation states and mineral solubilities. A whole-core squeezer was modified to operate in situ to capture high-resolution porewater in the top few cm (Sayles and Dickinson 1991). This and subsequent similar devices led to important studies on carbonate chemistry in Atlantic Ocean sediments (Martin et al. 2000). A rapid equilibration in situ peeper system employed passive diffusion of porewater through filters over several days and was able to measure spatial variability and heterogeneity due to bioturbation/irrigation (Aller et al. 1998). We have built on some of these ideas to develop our in situ porewater sampler. Notably, we have focused on collecting high-resolution porewater profiles from the top few cm below the SWI through 30 cm, as well as conducting the first carbonate dissolution rate experiments, in situ within deep-sea sediments.

The traditional method of collecting porewater, via sediment core collection and on-board filtration or centrifugation, allows the porewater to interact with sediment grains as the collected core travels through the water column to an environment with decreased pressure and often increased temperature. Temperature changes can cause certain ions to adsorb or desorb to sediment particles, such as the observed increases of K and Cl and decreases of Mg and Ca (Bischoff et al. 1970). It was later discovered that if sediment cores are brought down to in situ temperatures before porewater extraction, the enrichments or depletions can be reversed (Bischoff and Sayles 1972). However, the pressure artifact cannot be reversed and causes the saturation state of $CaCO_3$ to rise, resulting in carbonate precipitation within the core, lowering both porewater alkalinity (Murray et al. 1980) and dissolved inorganic carbon (DIC) (Sauvage et al. 2014). $CaCO_3$ is more likely to precipitate onto existing nucleation sites, especially existing carbonate grains, rather than spontaneously in solution. Therefore, even though isolated porewater will experience the same pressure and temperature changes as sediment cores, the lack of nucleation sites in the isolated porewater will hinder $CaCO_3$ precipitation. Sauvage et al. 2014 demonstrated that this sediment-induced artifact was a function of the time a recovered core spent at low pressure prior to porewater extraction, but there are many other factors that could affect the magnitude of this alkalinity artifact, as we show here.

To investigate deep-sea porewater chemistry and conduct $CaCO_3$ dissolution experiments, we built *S*ampling *I*n situ *P*orewate*R* (SIPR) to accomplish the following goals:

1. Filter deep-sea porewater in situ, thereby avoiding artifacts induced by pressure and temperature changes during sediment core recovery when water remains in contact with sediment grains.
2. Capture centimeter-scale resolution porewater profiles of carbonate chemistry parameters, among other constituents, specifically focused near the SWI.
3. Perform isotopically labeled calcite dissolution rate experiments in situ within sediment porewater.

Materials and procedures

Overview of in situ porewater sampling

The overarching purpose of SIPR is to separate porewater from sediments in situ, thereby avoiding recovery artifacts. SIPR was designed to be attached to a multicorer, a standard oceanographic tool. As described below, all SIPR components mount onto a multicorer, preserving the ability to collect cores as well as deploy SIPR for in situ porewater collection. Any ship that can deploy a multicorer (4 or 8 unit corer) can thus deploy SIPR.

Two different SIPR designs enter the sediment as the multicorer frame hits the seafloor: the "needles" and the "blades" (Fig. 1). Blades and needles are mounted on the multicorer Spyder, the inner part of the multicorer which drives the core tubes into the sediment under normal operation. Shortly after inserting the needles or blades into the sediment, porewater is drawn through filters from various depth horizons from 0 (SWI) to as deep as 30 cm.

The basic flow of operations is as follows (Fig. 2): multicorer is lowered to the seafloor from a cable attached to the ship; needles and blades are inserted into sediment; syringes are triggered via computer-controlled burn wire to draw porewater through filters and into a storage coil; after drawing porewater, a pinch mechanism (also fired by burn wire) prevents further suction before the device is removed from seafloor; multicorer is lifted from seafloor and received on-board where porewater samples are allocated for analyses or stored for at-home measurements. Time between multicorer recovery and partitioning of samples is less than 5 h. Table 1 provides descriptions and part numbers for all purchased parts; Table 2 provides descriptions for custom-made parts.

The Ocean Instruments MC-800 has eight positions available for core attachment. We use four slots for needles and/or blades and the other four slots for standard multicorer tubes. Thus, during one deployment, porewater is collected in situ and cores obtained for ex situ porewater extraction. Each draw from either blades or needles collects eight samples from separate depths. Each blade or needle collects porewater from a place on the seafloor that is ~ 50 cm away from the next blade or needle. Therefore, porewater samples from one deployment represent spatial variability within about 1.5 m^2 of the seafloor.

Needles

The needles are individual polycarbonate cylinders, 0.25 cm inner diameter, 20 cm long, that hold a Rhizon filter stick inside a pointed tip with 1-cm-tall open windows (Fig. 3a,d). The Rhizon stick is secured inside the needle by an o-ring seal. Eight needles reside on one platform, and each needle can be adjusted in height, with a range of 1 cm below SWI to 20 cm deep. These needles resemble the harpoon used by Sayles et al. (1976), except each needle draws only one sample and depth resolution can be focused near the SWI.

Blade

The blade is a SIPR filter system that was designed as a second method to collect porewater with the added benefit that it can also be used to conduct in situ carbonate dissolution experiments. The blade is made from Delrin plastic 1 cm thick and 30 cm wide. "Window" openings are machined into both sides, directly opposite each other, at varying depths to hold

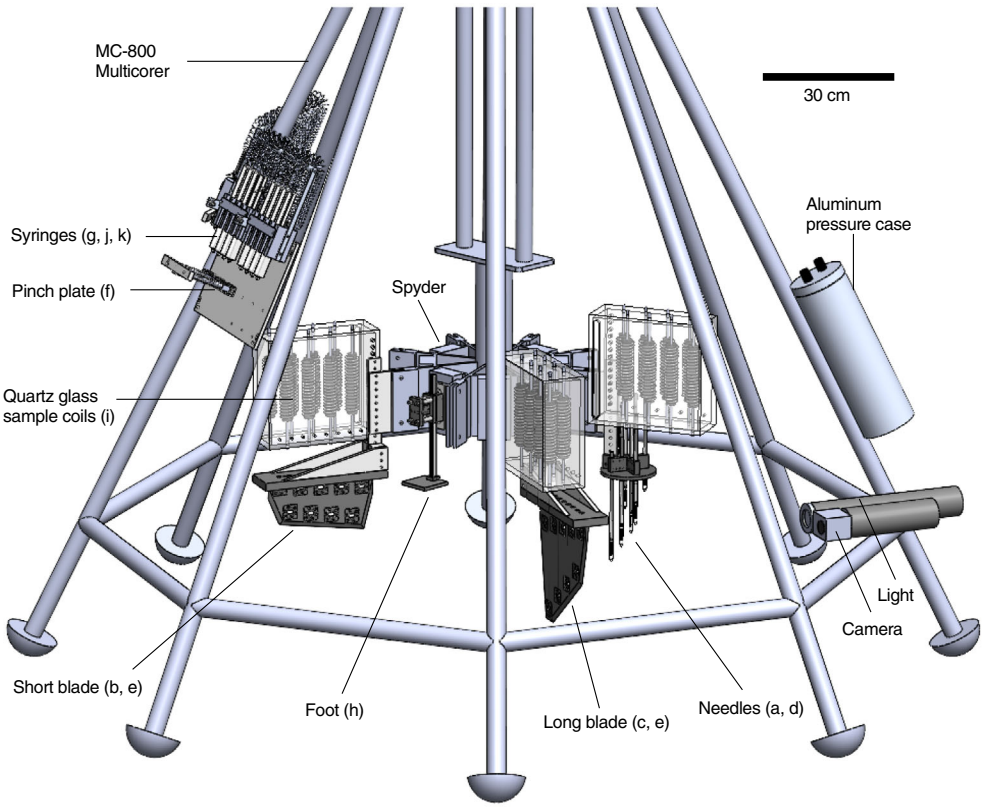

Fig. 1. SIPR assembled on multicorer. Letters correspond to those in Fig. 3. Not shown are core tubes attached to every other slot on Spyder, or lead bricks that help drive the Spyder into the sediment.

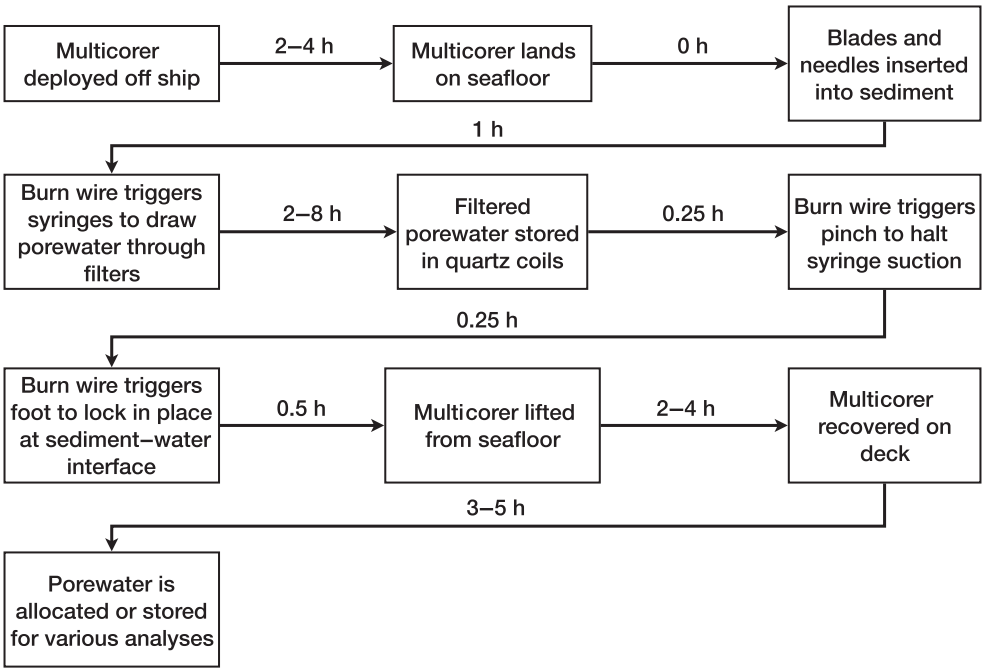

Fig. 2. Flow chart of SIPR operations. Timing intervals are programmed into the computer sent down with the multicorer.

Supor filters (0.45 μm), secured and sealed with two o-rings and a frame held against the filter with six screws (Fig. 3b,c,e). Blades come in two lengths, the short blade has windows down to 11 cm, with filters spaced 0.5 cm apart near the SWI; the long blade has filter windows as deep as 30 cm below the SWI. Like the needles, the blade filter window openings are

Table 1. Purchased parts.

Part	Description	Part no.	Vendor
Multicorer	Eight sample tubes with an effective penetration of > 45 cm	MC-800	Ocean Instruments
Rhizon filters	0.15 μm pore size, 5 cm porous part, flat tip, 2.5 mm OD, glass fiber strengthener, PE/PVC tubing 12 cm, female luer	19.21.23F	Rhizosphere
Supor filters	0.45 μm pore size, 25 mm	60172	Pall
Polypropylene net filter	25 μm pore size, 25 mm	PP2502500	Millipore
^{13}C calcite	Sieved to 18–53 μm. Geometric surface area of 0.064 $m^2\ g^{-1}$	SKU 492027	Sigma Aldrich
NaF	Sodium fluoride powder	201154-5G	Sigma Aldrich
PVDF (Kynar) tubing	0.0625″ ID, 0.125″ OD	51105K21	McMaster-Carr
Tygon tubing	0.125″ ID, 0.25″ OD	F-4040-A	Tygon
Silicon tubing	0.125″ ID, 0.188″ OD	06422-04	Cole-Parmer
Syringes	2.5 cm″ ID, 60 mL capacity	628426	Codan (Sweden)
Syringe springs	7″ long extension spring, 4.165 lbs per inch	7749N879	McMaster-Carr
O-ring (inner)	Buna-N-019	9452K73	McMaster-Carr
O-ring (outer)	Buna-N-022	9452K76	McMaster-Carr
Burn wire	7 × 7 stainless steel nylon-coated wire. 40 lb test	CM49-40T-A	AFW
Heat-shrink tubing	25′ length, 0.06″ ID	7856K41	McMaster-Carr
Arduino Uno computer Rev3	Micro-controller with Adafruit data logging shield, mechanical relay shield, custom circuit board	A000046	Arduino
Tilt meter	ADXL335-5V ready triple-axis accelerometer to record angle in *x*, *y*, *z* directions and acceleration	163	Adafruit
Camera and light package	Benthic underwater camera and light, rated to 2800 m	N/A	Group B Inc.

Table 2. Custom-built parts fabricated at USC.

Part	Material	Description
Needles	Polycarbonate plastic	0.25 cm ID, 20 cm long, 1 cm diameter, tip with 1 cm tall sample port
Blade	Delrin plastic	Short blade: 11 cm long, 30 cm wide, 1 cm thick
		Long blade: 30 cm long, 30 cm wide, 1 cm thick
Sample coils	Quartz glass	0.5 cm ID, 0.7 cm OD. 30 mL capacity
Foot	Delrin plastic	9 × 9 × 1.25 cm rectangular plate
Pressure case	Aluminum	47 cm long cylinder 15 cm OD with walls 2.54 cm thick, can withstand pressure > 4000 m

1 cm tall, thus defining the vertical resolution per sample. For both the needles and blades, sample windows were spaced such that porewater drawn would not overlap with adjacent samples. Both needles and blades are fitted into a retaining plate that (1) connects the blade to the multicorer, (2) provides some resistance to overpenetration, and (3) prevents or slows overlying water (OLW) from channeling down toward filter windows.

Carbonate dissolution experiments

In addition to collecting porewater for natural porewater profiles, we also built the blades to conduct in situ carbonate dissolution experiments within the sediment column. To conduct a dissolution experiment, the blade filter is replaced by a heat-sealed filter "sandwich" containing 2–10 mg of isotopically labeled $Ca^{13}CO_3$ (calcite) grains. Labeled calcite grains were purchased from Sigma-Aldrich and wet sieved to 18–53 μm using 18.2 MΩ DI water. Porewater is drawn past these grains and, accounting for isotopic exchange, an enriched $\delta^{13}C$ DIC signal will appear if dissolution occurs. A model translating $\delta^{13}C$ ratios into gross and net $CaCO_3$ dissolution rates is the topic of another study (H. A. Barnhart unpubl.). The actual amount of carbonate dissolved is small enough that DIC and alkalinity are unchanged by the process, allowing these samples to still be used for defining porewater gradients.

Sample coils

Porewater is drawn through the blade or needles, then through a short piece of polyvinylidene flouride (PVDF) Kynar tubing (< 10 cm) into quartz glass coils (Fig. 3i). Quartz glass (0.5 cm ID, 0.7 cm OD) was chosen because it does not allow gas diffusion and introduces no artifacts in DIC, alkalinity, or silica. Tests were conducted in the lab to ensure that these constituents did not change in seawater incubated for 6–12 h in the coil. The inner diameter (0.5 cm) of the quartz coil was chosen to minimize mixing between fill water and porewater during sample draw. Coils are designed to conserve space and provide some structural support for otherwise fragile tubing. Each set of quartz coils is secured in a clear polycarbonate box for additional security. The coils have an internal volume of 30 mL. For samples without labeled calcite grains in filters, that is, "natural samples," the entire 30 mL is removed, homogenized, then partitioned for analyses. For samples with labeled calcite grains in filters, that is, "dissolution experiments," aliquots of 7–8 mL are removed in sequence, to capture a time sensitive signal of $\delta^{13}C$ during dissolution.

Pinch

Once triggered, there is no mechanism to stop suction from the syringe until it hits a set screw at 55 mL, even if the device is removed from the sediment. Therefore, a pinching apparatus was designed to prevent suction before the multicorer is lifted from the seafloor (Fig. 3f). The pinch is a spring-loaded guillotine apparatus, held up by a burn wire, that pinches eight short lengths of flexible tubing closed at a programmed time. These short pieces of tubing are part of the continuous draw stream, so when they are pinched shut, there can be no more suction.

Syringes

The plungers of 60-mL Codan syringes were modified with an eye bolt attached to springs (Fig. 3g,j,k). The syringes and springs are mounted into a custom-machined rack. The rack holds the springs in the extended position, acting to pull the plungers up. The plungers are held down by a piano hinge that is secured by a burn wire. At a programmed time, the burn wire releases the hinge and allows the springs to pull up the plungers. This is when suction begins and porewater is drawn through SIPR filters. The negative pressure created by suction is at most 30 psi (21 dbar), which is negligible in comparison to water pressure at our sites, ranging from 1279 to 3256 dbar, and therefore does not affect the saturation state of calcite in a meaningful magnitude. These syringes were chosen because they work well in deep-sea applications, for example, benthic landers (Kononets et al. 2021).

Foot

A "foot" was designed to initially estimate the location of the SWI in relation to the multicorer frame, and thereby the depth of the SIPR windows. The foot has a rectangular Delrin plate attached to a geared shaft that is free to slide relative to the multicorer (Fig. 3h). This plate gently rests on the seafloor when the multicorer lands (confirmed by the camera), then locks in place via burn wire by the spring-loaded pressure of a

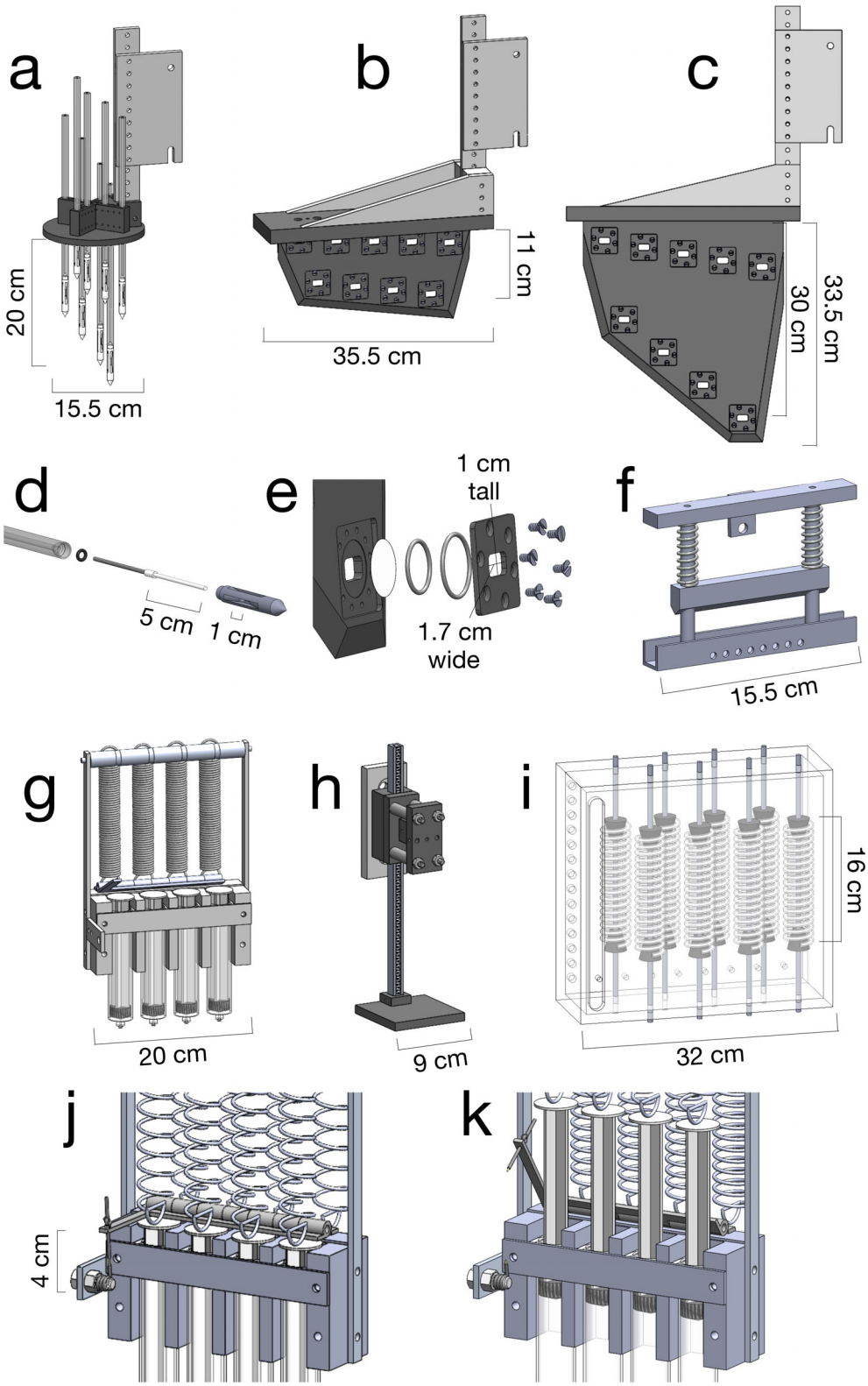

Fig. 3. SIPR components. (**a**) Needles, (**b**) short blade, (**c**) long blade, (**d**) exploded needle showing Rhizon filter and o-ring, (**e**) exploded blade filter showing Supor filter with polypropylene net filter, two o-rings, and six screws holding down window covering, (**f**) pinch plate, (**g**) syringe rack showing 60-mL syringes with springs to pull plungers, (**h**) foot to record SWI position, (**i**) quartz coils in protective box, (**j**) syringe rack detail showing burn wire holding down the piano hinge that restrains the syringe plungers, (**k**) syringe rack detail showing burn wire released and syringe plungers pulled up by springs.

locking gear. Once back on deck, the position of the foot is measured relative to the multicorer which defines how deep each of the SIPR windows were relative to the SWI. Two of these devices are attached on opposite sides of the multicorer to establish the position of the SWI and determine if the seafloor is sloped.

Tubing and fittings

The tubing that connects SIPR parts is designed to minimize internal volume, prevent the diffusive loss of CO_2, and avoid contamination of measured constituents. Minimal lengths of PVDF tubing are used between the blade/needles and quartz coils; PVDF is used between quartz coils and pinch plate; silicon tubing in the pinch plate; and Tygon between pinch plate and syringes. Luer lock two-way valves and barbs are used to connect tubing.

Computer and pressure case

An aluminum pressure case (10 cm ID, 47 cm length, rated to 10,000 m) holds an Arduino computer and 12 1.5-V D batteries (2 parallel sets of 6 batteries in series for 9 V output). The computer controls a bank of relays (on a circuit board that we fabricate) that fire burn wires at specified times. A tilt meter on the electronics package records changes in the *x*, *y*, and *z* dimensions, informing if the ship's cable ever displaced the multicorer while sitting on the seafloor for 6–12 h. The burn wire program is set prior to deployment, allowing for the time to get the multicorer to the seafloor (typically deployed at 40 m min^{-1}). Because the pressure case is the ground for the electrical circuit, it is mounted on the multicorer with care to isolate it with rubber sheeting so it does not ground to the frame.

Camera

A camera and light are also attached to the multicorer for several purposes: (1) observe position of blades and needles on the SWI, (2) record syringe draw rates, and (3) observe potential disturbance of multicorer during deployment. The Group B Inc. camera and light are housed in their own pressure cases that are rated to 2800 m water depth. Therefore, the camera and light can only be deployed up to this depth, even though the computer pressure case and multicorer can be deployed deeper. The camera and light package can be programmed to turn on and off at specified times and can record up to 6 h of video footage. As shown in Fig. 1, we attach the camera and light low on the multicore to capture both syringe draw rate and insertion of the blades and needles into sediment.

Fill water

The tubing and sample coils must be filled with a liquid prior to deployment to prevent tubing collapse as a result of deep ocean pressures. This "fill water" must have a chemical tracer to distinguish between fill water and porewater, as the waters will inevitably mix during collection. Fill water should have carbonate parameters somewhat similar to the sample, minimizing error when correcting for mixing. Here, we have spiked surface seawater with fluoride (starting concentration of 1.3 ppm F^-, spiked to 10 ppm F^-) and measured its dilution using a fluoride electrode. The [F^-] in a mixed sample determines how much fill water is present, and the other measured constituents can be corrected with a two-endmember mixing equation. As demonstrated by mixing experiments in the lab at typical flow rates (Fig. 4), porewater with < 1% fill water is collected beyond the 6-mL closest to the fill water–sample water interface.

Burn wire

We use burn wires to actuate autonomous deep-sea operations. A single wire consists of a nylon-coated stainless-steel fishing leader (40 lb test) covered in heat-shrink tubing for added abrasion resistance. A small section (~ 2 mm) of the coating is removed at the desired burn location, exposing the bare wire to seawater. When the batteries in the pressure case are programmed to fire, the resulting current is sufficient to corrode the wire. The circuit is completed through seawater when electrons leave the steel (producing Fe^{+2}) and travel through seawater to the aluminum pressure case, which serves as the ground. The exposed steel corrodes in approximately 2 min and releases whichever piece it held. Figure 3 shows an example of burn wire holding down syringes (Fig. 3j) and then, upon corrosion (Fig. 3k), allowing the springs to pull up syringe plungers.

Maintaining seafloor position

If the multicorer is jostled or in any way disturbed by the ship's cable during a deployment, the blades and needles will move and compromise sample integrity. To mitigate potential disturbance, an extra 5–10 m of cable is paid out after the multicorer has landed. A Benthos glass float is attached 20 m above the multicorer to help float the cable so it does not get tangled on the multicorer. In addition, we devised a simple "stiff arm" consisting of a 2.54-cm-diameter 3-m-long polyvinyl chloride (PVC) pipe attached to the cable immediately above the Benthos float via hose clamps. The float keeps the cable off the multicorer and this stiff arm keeps the cable from wrapping around the float. In addition, dynamic positioning on the R/V Sally Ride (the ship on which we made our deep-sea deployments) maintained lateral position within 150 m^2 (< 15 × 10 m in latitude and longitude) for up to 12 h. During deployments described in this paper, we were subject to 0.5–1.5 m waves and winds 5–20 knots.

Validation of methods

Porewater draw depth

Windows on the blade were spaced such that 60 mL of porewater (the maximum volume drawn), centered in the window, would not overlap with adjacent windows. By drawing 60 mL (even though collecting only the last 30 mL for

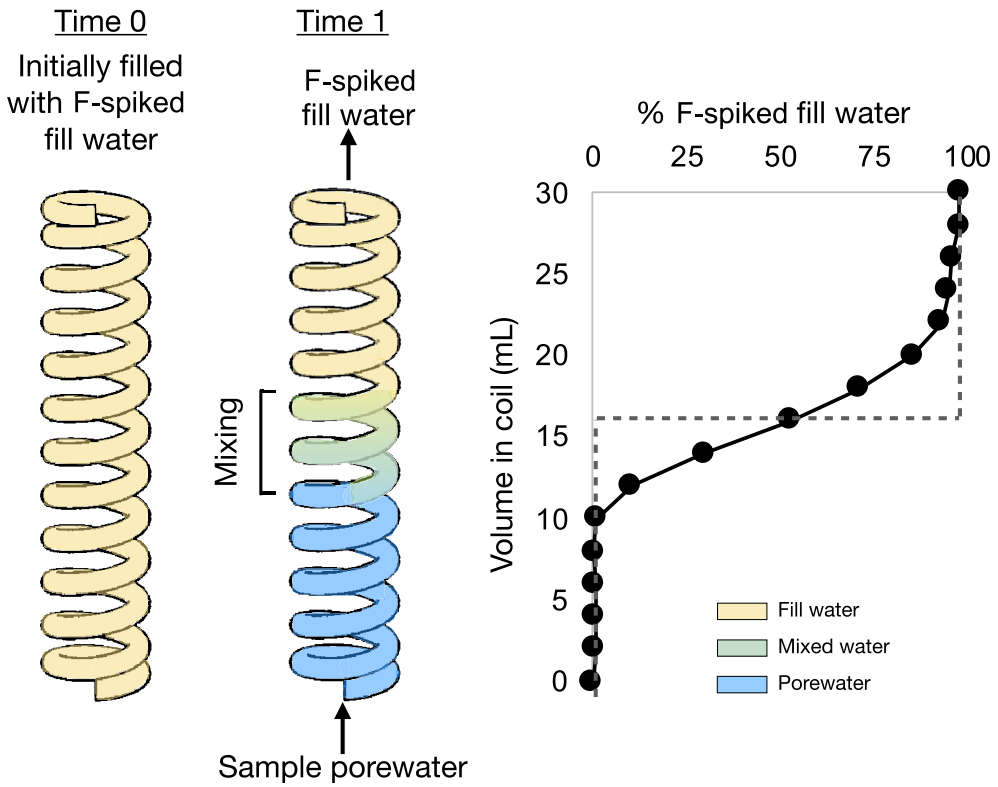

Fig. 4. Mixing experiment in sample coil initially filled with fluoride spiked seawater, with 16 mL sample porewater drawn into coil. The dashed line indicates hypothetical plug flow with no mixing. Solid circles are data points, and the solid line connects data points.

analyses), and assuming 74% porosity (lowest porosity at these field sites), the calculated radius of sample collection is 2.7 cm. The blade windows and needles are spaced 6 cm apart minimum, so overlapping sample volume is not likely. However, flow through muddy sediment is not likely to be perfectly uniform in all directions and is more likely to draw from shallower sediments where the porosity is higher. We conducted lab testing to confirm that SIPR windows draw porewater from the intended sediment horizon. Tests were conducted in the lab by inserting needles, blades, and Rhizon filters (inserted horizontally to mimic core Rhizon processing) into a container of muddy sediment. Porewater profiles from both SIPR methods indicated that needles and blades draw the same water as Rhizons, with the depth horizon centered around the midpoint of the filter. Bottom water entrainment into shallow SIPR windows will also contaminate samples. Lab testing with isotopically spiked OLW showed that when the retaining plate is securely placed on the sediment, bottom water entrainment is negligible.

OLW channeling/initial drawdown

Another concern was that during insertion of the blade or needles, OLW would be carried down into the sediments or move through channels opened during insertion. Needle and blade windows have internal volumes of 1 and 0.6 cm^3, respectively, that are exposed as multicorer travels through the water column. This volume is filled with OLW before insertion into sediment. A lab test was conducted by filling a bucket with mud and seawater, spiking OLW with ^{13}C and inserting the blade into the mud. By measuring the ^{13}C signal from sample DIC, we determined how much OLW is brought down in this process. As expected, this volume was at most 1 mL. Thus, we know that in addition to the fill water, there is also an extra $\sim$1 mL OLW that enters the window prior to sample draw. To obviate this contamination of our sample, we aim to draw more porewater than the 30 mL volume of the sample coil. That way, this OLW contamination is flushed out. If less than 30 mL was drawn, the first 6 mL of porewater was discarded to account for mixing of fill water and OLW with porewater (Fig. 4).

Flow rate

Knowing the porewater draw rate into the sampler helps us determine deployment timing and is also important in calculating dissolution rate from the labeled carbonate experiments. Flow rate is determined by either (1) dividing volume recorded on syringe by suction time or (2) observing the speed of syringe plunger movement via a camera. Syringes often draw the maximum volume, so the first method is not always viable, thus reported rates from Stas. 2 to 5 are those viewed

from the camera. Rates from Sta. 1 are from the first method of determining flow rate, as that site was deeper than the camera's depth rating of 3000 m. Both syringe travel and camera yield similar flow rates, as did lab testing which showed that volume draw vs. time is generally a linear function after 0.5 h. An example of flow rates from Sta. 2, characterized primarily by carbonate clays, is shown in Fig. 5. Natural samples have filters on both sides of the blade, whereas dissolution samples have a filter on only one side and therefore draw more slowly than natural samples. Obtaining a full draw (>50 mL) takes at least 2 h. Average natural sample flow rates are reported in Table 3. Flow rates vary among different sediment types and the rate is often fastest in the upper 5 cm, but otherwise does not scale with depth. The flow rates we found during deep-sea deployments in muddy sediments (Table 3) were comparable to those found during testing off the San Pedro Shelf (400 m). Clearly, the draw rate in sandy sediments was very fast compared to muds.

Field results and discussion

The tests described above validated that SIPR works as intended in the lab, and the following measurements verified the performance of SIPR in the field. Because of the low volume collected from SIPR (maximum 30 mL in sample coils), all analyses must be run on the smallest amount possible. Table 4 summarizes the analyses run and relevant instrument information. Total alkalinity was measured using the mvMICA system (X. Liu unpubl.), able to determine alkalinity on 1.5 mL of sample with a precision of 2 μM. mvMICA is novel in its low volume requirement, but it was built upon established methods (Liu et al. 2006, 2011, 2013; Wang et al. 2007).

Heterogeneity

It is possible for heterogeneity in natural sediment systems to drive differences in porewater profiles not due to any artifact or instrument malfunction. To test the extent that heterogeneity impacts SIPR profiles, we utilized the adjustable nature of the needles. At a test station in San Clemente Basin (1975 m water depth), all eight needles were set to the same depth (20 cm). The needles were laterally spaced 2 cm from one another and occupied an area of 24.4 cm^2. Aside from one needle that leaked (leaks are diagnosed by high % fill solution in sample water), the remaining seven needles contained an average dissolved silicate value of 292.6 μM with a standard deviation of 7.3 μM. This is the same value within error from blade windows at the same depth. The variability in [Si] values is only slightly higher than our analytical precision (± 2%, one standard deviation of replicates). These results confirmed that in situ samples drawn from the same depth yield similar concentration values. It also suggests that, at least in San Clemente Basin, any natural heterogeneity in porewater [Si] must be smoothed out by our sampling or does not exist. However, we do recognize that heterogeneity will exist in sediments, largely due to infaunal activity, but this was not observed in San Clemente Basin and would be expected to be less common at deeper sites further from coastal upwelling. We also recognize that heterogeneity in other constituents, such as carbonate parameters, may be greater than for dissolved [Si].

Sample depth

As is true with any porewater profile work, assigning depth to a particular sample is key to defining the profile shape. We have three independent methods of determining depth of the blade and needle windows:

1. **Relative depth:** The foot is designed to sit on, and thereby mark, the SWI. The foot is a physical method to compare where the blades and needles are in space, relative to the SWI. Upon recovery of the multicore, the location of the feet was measured to assign temporary depths and to ensure that the blades and needles were inserted into the sediment. There are 2 feet on the multicorer, so their

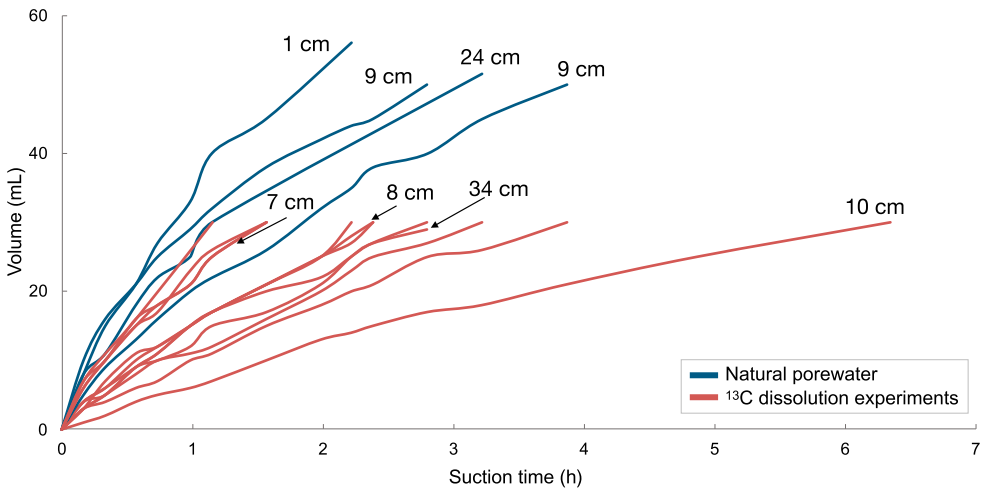

Fig. 5. SIPR flow rates at Sta. 2, as seen via camera. A subset of sediment depths is indicated.

Table 3. Stations visited on Cocos Ridge in November to December 2021. Sediment characteristics and SIPR draw rates reported.

Station #	Station coordinates	Water depth (m)	Sediment type	Porosity range (%)	Average SIPR flow rate (mL h^{-1})	Weight % $CaCO_3$ range
1	6°47.08′N, 88°15.65′W	3223	Low carbonate clay	84–94	7	0–18
5	6°35.99′N, 86°41.75′W	2911	Medium carbonate clay	81–93	6	10–33
2	5°57.48′N, 87°57.40′W	2650	Medium carbonate clay	78–88	13	57–64
3	5°10.17′N, 86°35.59′W	1630	High carbonate clay	74–83	70	75–81
4	4°48.72′N, 88°37.31′W	1274	Foraminiferal sand	74–80	3600	91–93

position relative to the frame is extrapolated to the blades and needles, providing relative depth of SIPR windows between multiple blades and needles.

2. **Visual depth:** The camera field of vision captures one blade to provide evidence of the depth of blade penetration. The video captures insertion of a blade into the sediment and shows if the multicorer was disturbed during the suction time. The multicorer was never displaced from the sediment in all nine deployments. From markings on the blade, the camera provides visual evidence of the penetration and thus the window depths.
3. **Chemical depth:** For each deployment, dissolved silicate [Si] profiles were compared between SIPR blades/needles and shipboard-processed cores filtered with Rhizons (Fig. 6). Cores have definite depth assignments due to the relatively gentle insertion of the multicorer into sediment and resulting interface preservation. Previous work with [Si] gives us confidence that shipboard-processed cores reflect accurate porewater gradients near the SWI (McManus et al. 1995; Berelson et al. 1997; Hou et al. 2019).

From three shipboard-processed cores, we generate an average [Si] porewater profile. The top 0–10 cm of core profiles was fitted with a linear, second, or third order polynomial (best fit). SIPR blades/needles were then shifted in depth, up or down, to minimize the difference in SIPR and core [Si], producing a "silica depth." Each blade/needle set must only have one depth offset by which all windows are shifted. On average, this [Si] adjustment in depth was $< \pm 1$ cm compared to relative depth. This [Si] depth adjustment of in situ samples does not change the magnitude of the concentration change, only the position relative to the SWI. After the [Si] depth correction, individual blades and needle sets collapse onto the core [Si] gradient (Fig. 6b).

We consider the chemical depth assignment to be the most accurate. Relative depth can be influenced by seafloor topography; visual depth only applies to half the blades or needles that fit in the field of vision. Most importantly, where we have camera evidence of blade penetration, the assigned chemical depths agree with visual depths.

We found a difference between in situ and ex situ dissolved [Si] deeper in the core (>10 cm; Fig. 6). The in situ dissolved [Si] profiles reach higher values than the ex situ core profiles. This offset is seen after we adjust core [Si] for a temperature correction (McManus et al. 1995). We do not have a ready explanation for this offset but have perhaps documented yet another pressure/temperature/precipitation artifact between in situ and ex situ porewater collection. Unless stated otherwise, reported sediment depths are in terms of this silica correction.

Table 4. Analyses performed on in situ collected porewater. Except for dissolved silicate, all analyses were run on-board.

Analysis	Instrument (reference)	Volume (mL)	Standard	Precision (one standard deviation of replicates)	Lab
DIC	Picarro Cavity Ring-Down Spectrometer (Subhas et al. 2015)	4	Dickson CO_2 reference material seawater	23 μmol kg^{-1}	Berelson (USC)
$\delta^{13}C$ of DIC	Picarro Cavity Ring-Down Spectrometer (Subhas et al. 2015)	4 (same water as DIC)	Optical calcite powder	0.15‰	Berelson (USC)
Total alkalinity	Minimal volume multiparameter inorganic carbon analyzer (mvMICA) (X. Liu et al. unpubl.)	1.5	Dickson CO_2 reference material seawater	2 μM	Byrne (USF)
pH	mvMICA (X. Liu et al. unpubl.)	1.5	N/A	0.001	Byrne (USF)
Dissolved silicate	Spectrophotometer (Hou et al. 2019)	1	Artificial seawater	2%	Berelson (USC)
Fluoride	Orion fluoride electrode (Rix et al. 1976)	1	TISAB	0.1 ppm	Adkins (Caltech)

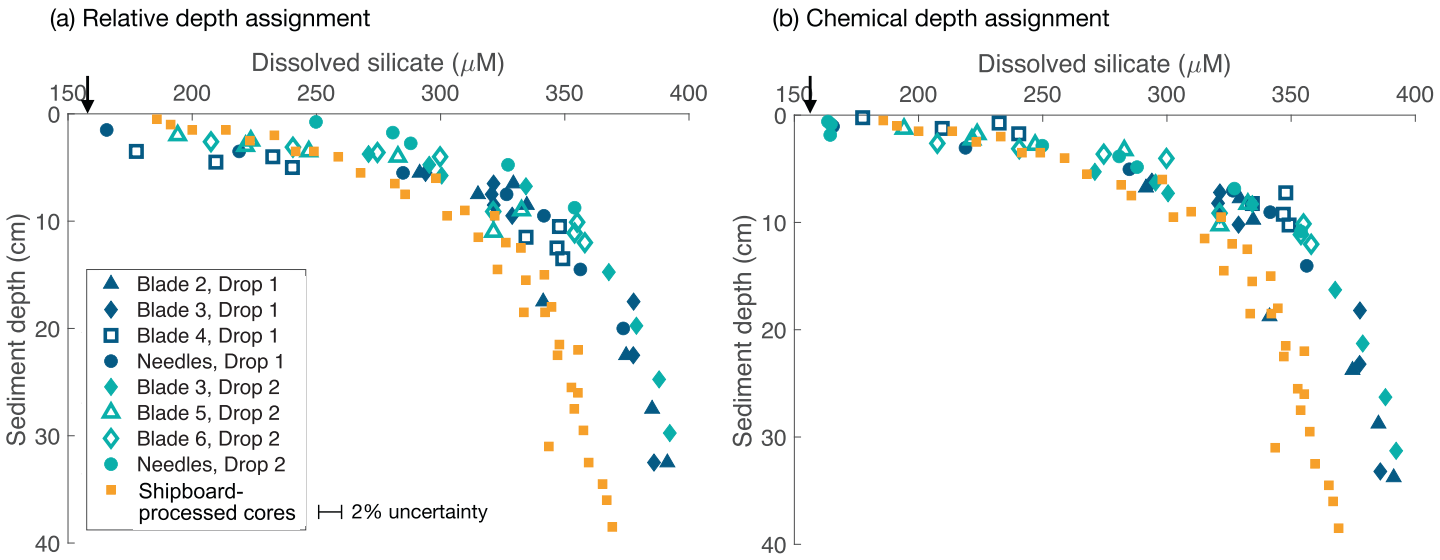

Fig. 6. Sta. 2 dissolved silicate from in situ porewater (blue) and ex situ shipboard-processed core porewater (yellow), before (**a**) and after (**b**) silica depth correction. Arrows denote CTD bottom water values. Different blue colors and symbols represent individual blades over two deployments, demonstrating the reproducibility of SIPR devices. Uncertainty of [Si] measurements is 2%.

In addition, [Si] can diagnosis bottom water entrainment into shallow SIPR windows. If a sample falls off the trend defined by the majority of data and has a lower [Si] value, that is, closer to bottom water, we assume that sample must have had channeling of bottom water into the sample window, and is therefore removed from further analyses.

Alkalinity in situ vs. cores

There is a known artifact that occurs when dissolved Ca^{2+} and CO_3^{2-} ions precipitate as $CaCO_3$ onto existing nucleation sites (for example, sediment grains) as pressure and temperature change during core recovery from deep water prior to porewater filtration (Murray et al. 1980; Sauvage et al. 2014). Due to this artifact, alkalinity is lowered in porewater extracted from cores processed on-board. Our data confirm this artifact and demonstrate how it impacts the profile gradient and structure (Fig. 7). This artifact not only reduces the maximum alkalinity value, but drastically changes the slope and shape of the profile, especially in the top few cm. Importantly, fluxes calculated from core profiles would be much lower than those from porewater collected in situ.

Alkalinity artifact vs. sedimentary $CaCO_3$

To investigate potential explanations for this alkalinity sampling artifact, the alkalinity loss from ex situ shipboard-processed cores relative to in situ porewater was compared to weight % $CaCO_3$ in sediments (Fig. 8). This comparison is made more robust by our range in weight % $CaCO_3$: between 1630 and 3223 m water depth, we collected sediments that range from 0 to 80 weight % $CaCO_3$. The magnitude of the artifact was quantified by taking the average of all SIPR points within 1 cm intervals, taking the average of all core points within 1 cm intervals, then calculating the % loss between SIPR and core values at each cm horizon. Weight % $CaCO_3$ was measured by sectioning cores at 1–2 cm intervals, grinding the sediment to a powder, then acidifying the sediment with 10% H_3PO_4 in an evacuated container to convert $CaCO_3$ to CO_2. This CO_2 was then measured on a Picarro Cavity Ring-Down Spectrometer.

Three potential mechanisms for alkalinity loss were examined in this study: (1) the effect of weight % $CaCO_3$ (higher weight % $CaCO_3$ has more potential for alkalinity loss by providing more nucleation sites onto which carbonate can

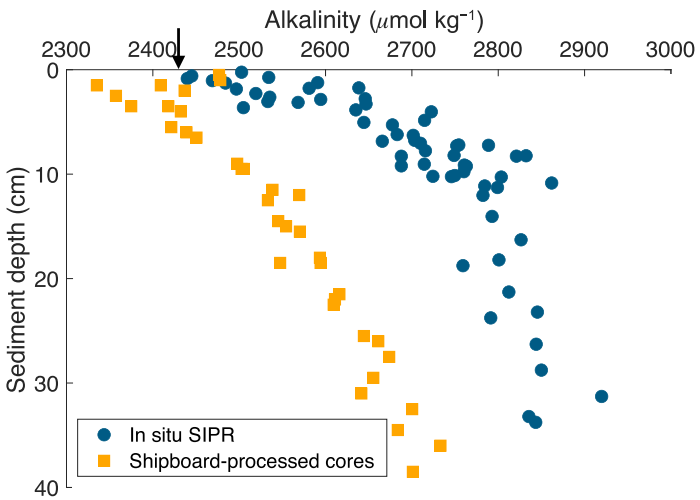

Fig. 7. Sta. 2 porewater alkalinity from in situ vs. ex situ (shipboard-processed cores) filtered porewater. SIPR points represent all blades and needles over two deployments. Arrow denotes CTD bottom water value. Error bars are smaller than size of point.

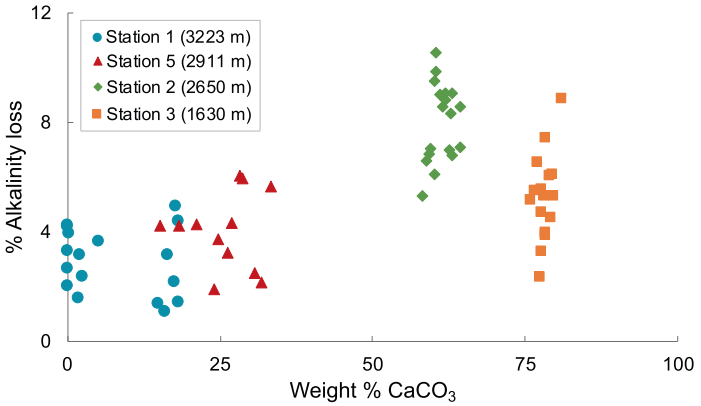

Fig. 8. Porewater alkalinity lost from shipboard-processed cores relative to in situ porewater vs. weight % $CaCO_3$ in sediment core samples. Data are binned for every 1–2 cm interval.

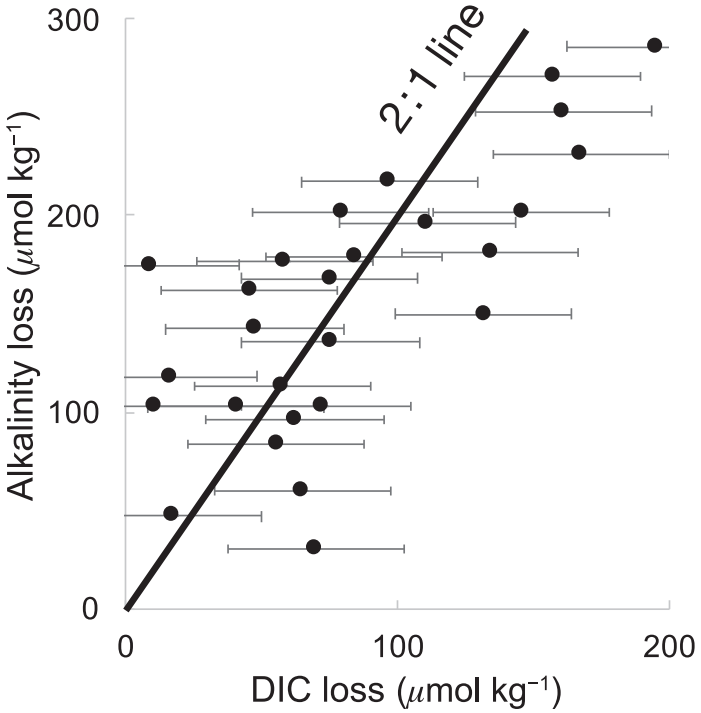

Fig. 9. Alkalinity and DIC loss (Δ) in shipboard-processed cores compared to in situ filtered SIPR porewater at all stations. Alkalinity : DIC 2 : 1 ratio line. Δ DIC uncertainty: ± 32.5 μmol kg^{-1}. Δ Alkalinity uncertainty: ± 2.8 μM.

precipitate); (2) the effect of water column depth (based on the known relationship between pressure, temperature, and the saturation state of carbonate); and (3) time between core recovery and processing (as found by Sauvage et al. 2014). Sites deeper than 2600 m (Stas 1, 2, and 5) exhibit a trend of more alkalinity loss with increased carbonate content. Contrary to the pressure artifact definition, Sta. 1, the deepest site, shows the smallest, albeit non-negligible, alkalinity artifact and it is the core with the lowest % $CaCO_3$. From 3200 to 2600 m, weight % $CaCO_3$ is positively correlated with % alkalinity loss in ex situ processed cores.

However, Sta. 3 at 1600 m has the highest weight % $CaCO_3$, yet has an average alkalinity artifact smaller than that at Sta. 2, where there is less sedimentary carbonate. Therefore, weight % $CaCO_3$ is not the only factor influencing alkalinity loss in cores; water column depth may also play a role, as could other sedimentary features and composition.

Last, we compared time between core recovery and processing to see if this impacted alkalinity. Sauvage et al. 2014 measured an average loss of 8.9% alkalinity in cores due to $CaCO_3$ precipitation after waiting 3–7 h to extract porewater, compared to cores processed in < 2 h. Our cores were placed in a cold van until they reached bottom water temperature. Three cores were processed for porewater at each station; the time between core recovery and Rhizon-processing ranged from 8 to 27 h. There was no systematic difference among the alkalinity profiles from three cores/station processed at different times. We believe that we do not see the same sampling time artifact as Sauvage et al. 2014 because our shortest wait-time is longer than their longest wait-time and this effect can only be seen within the first 2 h after recovery.

Alkalinity loss was also compared to DIC loss in cores relative to SIPR (Fig. 9). The premise being if carbonate precipitation were responsible for this artifact, an Alk : DIC (Δ) loss ratio of 2 : 1 would be diagnostic of this mechanism. Both alkalinity and DIC losses were calculated by taking the average of all SIPR points within 1 cm intervals and subtracting the average of all shipboard-processed core points for the same horizon. Although there is significant scatter in the data, possibly due to the relatively high uncertainty of our DIC measurements (± 23 μmol kg^{-1}), the average alkalinity loss/DIC loss is equal to 2.2, consistent with the signal expected from carbonate precipitation.

Assigning mechanistic controls of this artifact is beyond the scope of this work, but we believe this is the first study to show a large range of this alkalinity artifact as a function of deep-sea sediment type and depth. Weight % $CaCO_3$ and water column depth are demonstrated as important factors contributing to artifact magnitude; as others have suggested (Murray et al. 1980; Sauvage et al. 2014), carbonate precipitation during core recovery is the likely driver.

In situ carbonate dissolution experiments

At all stations, we conducted the first in situ carbonate dissolution rate experiments in sediments. Isotopically labeled calcite grains were placed in blade windows for porewater to be drawn past. A measured enrichment of $\delta^{13}C$ in DIC comes from two processes: isotopic exchange at the solid–solution interface and calcite dissolution. The first necessary measurement is to define the ambient $\delta^{13}C$ DIC profile (Fig. 10a) in the absence of any labeled carbonate. As porewater is drawn past labeled calcite grains, isotopic exchange between the

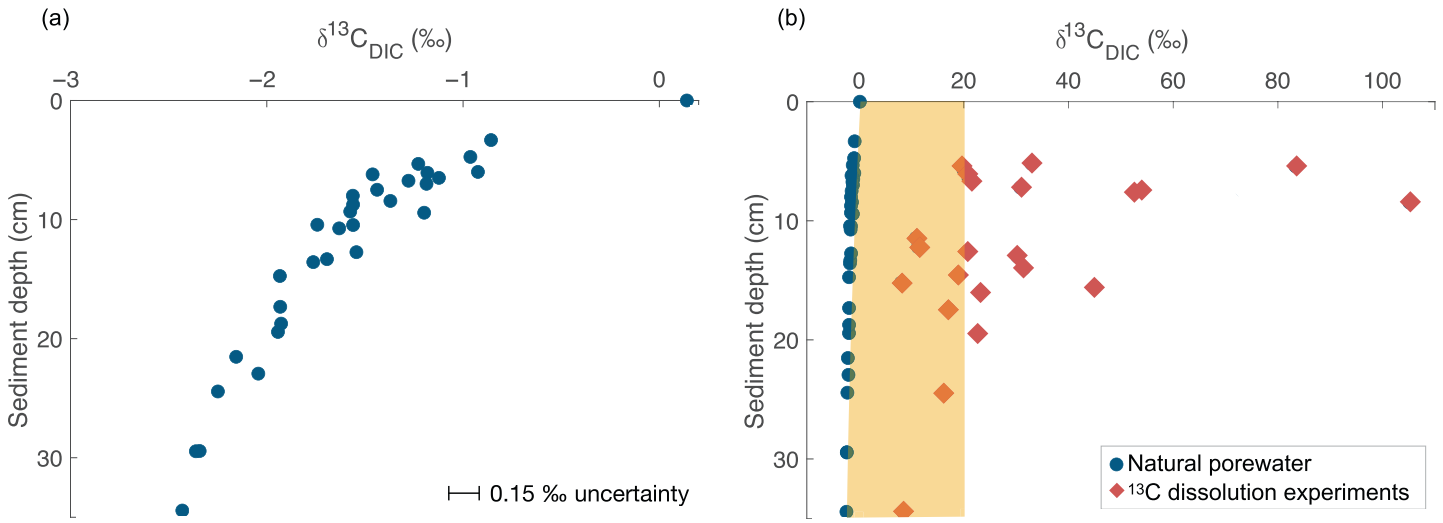

Fig. 10. Sta. 5 $\delta^{13}C$ of DIC. (**a**) Ambient in situ profile, and (**b**) ambient profile and results of in situ calcite dissolution experiments. Dissolution experiments shown (diamonds) are the aliquot farthest from the porewater–fill water interface. Yellow band indicates potential range of isotopic exchange signal. Note change in *x*-axes. Sta. 5 has OLW with $\Omega_{calcite} = 0.89$.

grains and adjacent porewater can occur independently of dissolution. Such isotopic exchange signals have been documented in benchtop experiments in supersaturated seawater (Subhas et al. 2015). The relative contributions of $\delta^{13}C$ from isotopic exchange and dissolution is currently being studied (H. A. Barnhart unpubl.). However, based on in situ dissolution experiments in supersaturated porewater, we estimate the effect of isotopic exchange is 10–20‰. An example from Sta. 5 (OLW $\Omega_{calcite} = 0.89$) shows significant enrichment relative to ambient $\delta^{13}C$ beyond the exchange estimate, indicating a contribution to the $\delta^{13}C$ signal from net carbonate dissolution (Fig. 10b). This occurs at the highest magnitude in the top 8 cm, likely where sediment is oxygenated, evidence of aerobic respiration-driven dissolution (Emerson and Bender 1981; J. E. P. Cetiner unpubl.). Dissolved manganese is depleted in these porewaters from the SWI to 8 cm (F. J. Pavia pers. comm.), indicative of the oxygen penetration depth. These results show that in situ dissolution experiments are a viable method for quantifying carbonate dissolution rates in sediments and qualitatively defining depth of dissolution.

Summary

SIPR was built to filter porewater from deep-sea sediments in situ, avoid sampling artifacts associated with traditional core recovery methods, and obtain high-quality samples for accurately characterizing porewater carbonate chemistry (DIC, $\delta^{13}C$ of DIC, Total Alkalinity, and pH). SIPR was successfully deployed nine times on and adjacent to the Cocos Ridge in the eastern equatorial Pacific, from 1300 to 3200 m, filtering porewater from sediment types ranging from low to high carbonate clay and foraminiferal sand. In comparing alkalinity profiles from in situ and ex situ shipboard-processed cores, the ex situ porewater exhibits a significant reduction in alkalinity, attributed to carbonate precipitation in cores, consistent with the ratio of alkalinity to DIC loss of 2.2. This artifact leads to a large difference in the steepness of the gradient (dC/dz) of in situ vs. ex situ profiles. This difference in gradient slope and shape will have profound impacts on the calculated fluxes of carbonate parameters from deep-sea sediments. We also established that this artifact (loss of 1–10% alkalinity) is a consequence of sediment % $CaCO_3$ and the water depth from which cores were processed ex situ.

Comparison to existing methods

Traditional methods for collecting deep-sea porewater include filtering from cores using Rhizons, centrifugation, and whole-core squeezers. Compared to these methods, SIPR is more time-intensive in both preparation and deployment: 20–24 person-hours for cleaning, blade/needle prep in lab, and deck prep (attaching all parts to multicorer, setting up electronics), and 6–18 h total deployment time. Despite these time constraints, it is clear that in situ porewater collection is necessary to generate high-resolution and accurate porewater profiles for carbonate species.

Comments and recommendations

SIPR was built with a future application for trace metals in mind, hence every surface that touches the porewater is metal-free. The multicorer and parts attaching SIPR to the multicorer are metal, but porewater is never in contact with these surfaces. Porewater is filtered through a Supor filter, pulled through Delrin plastic (blade) or polycarbonate sheathing

(needle), drawn through plastic tubing, and stored in quartz glass sample coils. Sample coils could be fabricated from plastic for trace metal applications, so long as there is no need to measure gas species. Further testing would need to be conducted to ensure these surfaces remain trace metal clean after acid washing, for example. Other work has clearly documented the sampling artifact of additional constituents besides carbonate species, such as O_2 (Glud et al. 1994), the nitrogen system (NH_4^+, NO_3^-, NO_2^-) (Aller et al. 1998), and dissolved organic matter (Hall et al. 2007), all of which would therefore require in situ filtration to obtain the most accurate porewater profiles, and for which SIPR could be adapted and deployed. SIPR would also be suitable for anoxic environments, as the quartz sample coils are gas impermeable and allow for separation between porewater (anoxic) and fill water (oxic). In addition to deep-sea studies, SIPR has potential for coastal applications as well. In sandy sediments, it is difficult to collect full cores due to the resistance to core penetration in sands. We demonstrated that SIPR is capable of collecting in situ porewater from sands up to 35 cm deep at Sta. 4 (data not shown). SIPR has a water column depth constraint set by the pressure case, which was built for use with the Alvin submersible and rated to 10,000 m.

In summary, through 3 yr of testing, we have developed a unique oceanographic instrument that will serve to further benthic chemistry research by providing tens of milliliters of artifact-free, in situ filtered porewater for carbonate chemistry constituents, among other applications. Pairing in situ porewater profiles with other in situ techniques (for example, pH and O_2 microprofiling, benthic chambers, eddy correlation studies) could lead to deeper understanding of carbonate dissolution on the seafloor.

Data availability statement

All data used in this paper are presented in the figures. Data sets are available upon request.

References

Adkins, J. F., J. D. Naviaux, A. V. Subhas, S. Dong, and W. M. Berelson. 2021. The dissolution rate of $CaCO_3$ in the ocean. Ann. Rev. Mar. Sci. **13**: 1–24. doi:10.1146/annurev-marine-041720-092514

Aller, R. C., P. O. J. Hall, P. D. Rude, and J. Y. Aller. 1998. Biogeochemical heterogeneity and suboxic diagenesis in hemipelagic sediments of the Panama Basin. Deep Sea Res. Part I **45**: 133–165. doi:10.1016/S0967-0637(97)00049-6

Archer, D., H. Kheshgi, and E. Maier-Reimer. 1998. Dynamics of fossil fuel CO_2 neutralization by marine $CaCO_3$. Global Biogeochem. Cycl. **12**: 259–276. doi:10.1029/98GB00744

Archer, D., and others. 2009. Atmospheric lifetime of fossil fuel carbon dioxide. Annu. Rev. Earth Planet. Sci. **37**: 117–134. doi:10.1146/annurev.earth.031208.100206

Berelson, W. M., D. E. Hammond, and K. S. Johnson. 1987. Benthic fluxes and the cycling of biogenic silica and carbon in two southern California borderland basins. Geochim. Cosmochim. Acta **51**: 1345–1363. doi:10.1016/0016-7037(87)90320-6

Berelson, W. M., and others. 1997. Biogenic budgets of particle rain, benthic remineralization and sediment accumulation in the equatorial Pacific. Deep Sea Res. Part II **44**: 2251–2282. doi:10.1016/S0967-0645(97)00030-1

Berelson, W. M., W. M. Balch, R. Najjar, R. A. Feely, C. Sabine, and K. Lee. 2007. Relating estimates of $CaCO_3$ production, export, and dissolution in the water column to measurements of $CaCO_3$ rain into sediment traps and dissolution on the sea floor: A revised global carbonate budget. Global Biogeochem. Cycl. **21**: 1–15. doi:10.1029/2006GB002803

Bischoff, J. L., R. E. Greer, and A. O. Luistro. 1970. Composition of interstitial waters of marine sediments: Temperature of squeezing effect. Science **167**: 1245–1246. doi:10.1126/science.167.3922.1245

Bischoff, J. L., and F. L. Sayles. 1972. Pore fluid and mineralogical studies of recent marine sediments: Bauer depression region of East Pacific rise. J. Sediment. Res. **42**: 711–724. doi:10.1306/74d72617-2b21-11d7-8648000102c1865d

Blättler, C. L., J. A. Higgins, and P. K. Swart. 2019. Advected glacial seawater preserved in the subsurface of the Maldives carbonate edifice. Geochim. Cosmochim. Acta **257**: 80–95. doi:10.1016/j.gca.2019.04.030

Boudreau, B. P. 2013. Carbonate dissolution rates at the deep ocean floor. Geophys. Res. Lett. **40**: 744–748. doi:10.1029/2012GL054231

Dong, S., A. V. Subhas, N. E. Rollins, J. D. Naviaux, J. F. Adkins, and W. M. Berelson. 2018. A kinetic pressure effect on calcite dissolution in seawater. Geochim. Cosmochim. Acta **238**: 411–423. doi:10.1016/j.gca.2018.07.015

Dong, S., and others. 2019. Aragonite dissolution kinetics and calcite/aragonite ratios in sinking and suspended particles in the North Pacific. Earth Planet. Sci. Lett. **515**: 1–12. doi:10.1016/j.epsl.2019.03.016

Emerson, S., R. Jahnke, M. Bender, P. Froelich, G. Klinkhammer, C. Bowser, and G. Setlock. 1980. Early diagenesis in sediments from the eastern equatorial Pacific, I. Pore water nutrient and carbonate results. Earth Planet. Sci. Lett. **49**: 57–80. doi:10.1016/0012-821X(80)90150-8

Emerson, S., and M. Bender. 1981. Carbon fluxes at the sediment–water interface of the deep-sea: Calcium carbonate preservation. J. Mar. Res. **39**: 139–162.

Foster, G. L., and E. J. Rohling. 2013. Relationship between sea level and climate forcing by CO_2 on geological timescales. Proc. Natl. Acad. Sci. **110**: 1209–1214. doi:10.1073/pnas.1216073110

Froelich, P. N., and others. 1979. Early oxidation of organic matter in pelagic sediments of the eastern equatorial

Atlantic: Suboxic diagenesis. Geochim. Cosmochim. Acta **43**: 1075–1090. doi:10.1016/0016-7037(79)90095-4

Glud, R. N., J. K. Gundersen, B. B. Jørgensen, N. P. Revsbech, and H. D. Schulz. 1994. Diffusive and total oxygen uptake of deep-sea sediments in the eastern South Atlantic Ocean: in situ and laboratory measurements. Deep Sea Res. Part I **41**: 1767–1788. doi:10.1016/0967-0637(94)90072-8

Hall, P. O. J., J. Brunnegad, G. Hulthe, W. R. Martin, H. Stahl, and A. Tengberg. 2007. Dissolved organic matter in abyssal sediments: Core recovery artifacts. Limnol. Oceanogr. **52**: 19–31. doi:10.4319/lo.2007.52.1.0019

Hales, B., S. Emerson, and D. Archer. 1994. Respiration and dissolution in the sediments of the western North Atlantic: Estimates from models of in situ microelectrode measurements of porewater oxygen and pH. Deep Sea Res. Part I **41**: 695–719. doi:10.1016/0967-0637(94)90050-7

Higgins, J. A., and D. P. Schrag. 2012. Records of Neogene seawater chemistry and diagenesis in deep-sea carbonate sediments and pore fluids. Earth Planet. Sci. Lett. **357–358**: 386–396. doi:10.1016/j.epsl.2012.08.030

Hou, Y., D. E. Hammond, W. M. Berelson, N. Kemnitz, J. F. Adkins, and A. Lunstrum. 2019. Spatial patterns of benthic silica flux in the North Pacific reflect upper ocean production. Deep Sea Res. Part I **148**: 25–33. doi:10.1016/j.dsr.2019.04.013

Jahnke, R. A., D. B. Craven, and J. F. Gaillard. 1994. The influence of organic matter diagenesis on $CaCO_3$ dissolution at the deep-sea floor. Geochim. Cosmochim. Acta **58**: 2799–2809. doi:10.1016/0016-7037(94)90115-5

Jahnke, R. A., D. B. Craven, D. C. McCorkle, and C. E. Reimers. 1997. $CaCO_3$ dissolution in California continental margin sediments: The influence of organic matter remineralization. Geochim. Cosmochim. Acta **61**: 3587–3604. doi:10.1016/S0016-7037(97)00184-1

Kononets, M., and others. 2021. In situ incubations with the Gothenburg benthic chamber landers: Applications and quality control. J. Mar. Syst. **214**: 103475. doi:10.1016/j.jmarsys.2020.103475

Liu, X., Z. A. Wang, R. H. Byrne, E. A. Kaltenbacher, and R. E. Bernstein. 2006. Spectrophotometric measurements of pH in-situ: Laboratory and field evaluations of instrumental performance. Environ. Sci. Technol. **40**: 5036–5044. doi:10.1021/es0601843

Liu, X., M. C. Patsavas, and R. H. Byrne. 2011. Purification and characterization of meta-Cresol Purple for spectrophotometric seawater pH measurements. Environ. Sci. Technol. **45**: 4862–4868. doi:10.1021/es200665d

Liu, X., R. H. Byrne, L. Adornato, K. K. Yates, E. Kaltenbacher, X. Ding, and B. Yang. 2013. In situ spectrophotometric measurement of dissolved inorganic carbon in seawater. Environ. Sci. Technol. **47**: 11106–11114. doi:10.1021/es4014807

Martin, J. B., M. Kastner, and H. Elderfield. 1991. Lithium: Sources in pore fluids of Peru slope sediments and implications for oceanic fluxes. Mar. Geol. **102**: 281–292. doi:10.1016/0025-3227(91)90012-S

Martin, W. R., A. P. McNichol, and D. C. McCorkle. 2000. The radiocarbon age of calcite dissolving at the sea floor: Estimates from pore water data. Geochim. Cosmochim. Acta **64**: 1391–1404. doi:10.1016/S0016-7037(99)00424-X

Martin, W. R., and F. L. Sayles. 2006. Organic matter oxidation in deep-sea sediments: Distribution in the sediment column and implications for calcite dissolution. Deep Sea Res. Part II **53**: 771–792. doi:10.1016/j.dsr2.2006.01.017

McManus, J., D. E. Hammond, W. M. Berelson, T. E. Kilgore, D. J. Demaster, O. G. Ragueneau, and R. W. Collier. 1995. Early diagenesis of biogenic opal: Dissolution rates, kinetics, and paleoceanographic implications. Deep Sea Res. Part II **42**: 871–903. doi:10.1016/0967-0645(95)00035-O

Murray, J. W., S. Emerson, and R. Jahnke. 1980. Carbonate saturation and the effect of pressure on the alkalinity of interstitial waters from the Guatemala Basin. Geochim. Cosmochim. Acta **44**: 963–972. doi:10.1016/0016-7037(80)90285-9

Naviaux, J. D., A. V. Subhas, N. E. Rollins, S. Dong, W. M. Berelson, and J. F. Adkins. 2019*a*. Temperature dependence of calcite dissolution kinetics in seawater. Geochim. Cosmochim. Acta **246**: 363–384. doi:10.1016/j.gca.2018.11.037

Naviaux, J. D., A. V. Subhas, S. Dong, N. E. Rollins, X. Liu, R. H. Byrne, W. M. Berelson, and J. F. Adkins. 2019*b*. Calcite dissolution rates in seawater: Lab vs. in-situ measurements and inhibition by organic matter. Mar. Chem. **215**: 103684. doi:10.1016/j.marchem.2019.103684

Reimers, C., R. Jahnke, and D. McCorkle. 1992. Carbon fluxes and burial rates over the continental slope and rise off central California with implications for the global carbon cycle. Global Biogeochem. Cycl. **6**: 199–224.

Rix, C. J., A. M. Bond, and J. D. Smith. 1976. Direct determination of fluoride in sea water with a fluoride selective ion electrode by a method of standard additions. Anal. Chem. **48**: 1236–1239. doi:10.1021/ac50002a044

Sauvage, J., A. J. Spivack, R. W. Murray, and S. D'Hondt. 2014. Determination of in situ dissolved inorganic carbon concentration and alkalinity for marine sedimentary porewater. Chem. Geol. **387**: 66–73. doi:10.1016/j.chemgeo.2014.06.010

Sayles, F. L. 1979. The composition and diagenesis of interstitial solutions-I. Fluxes across the seawater-sediment interface in the Atlantic Ocean. Geochim. Cosmochim. Acta **43**: 527–545. doi:10.1016/0016-7037(79)90163-7

Sayles, F. L. 1981. The composition and diagenesis of interstitial solutions-II. Fluxes and diagenesis at the water-sediment interface in the high latitude North and South Atlantic. Geochim. Cosmochim. Acta **45**: 1061–1086. doi:10.1016/0016-7037(81)90132-0

Sayles, F. L., T. R. S. Wilson, D. N. Hume, and P. C. Mangelsdorf. 1973. In situ sampler for marine sedimentary

pore waters: Evidence for potassium depletion and calcium enrichment. Science **181**: 154–156. doi:10.4213/mzm2562

Sayles, F. L., P. C. Mangelsdorf, T. R. S. Wilson, and D. N. Hume. 1976. A sampler for the in situ collection of marine sedimentary pore waters. Deep Sea Res. **23**: 259–264. doi:10.1016/0011-7471(76)91331-0

Sayles, F. L., and W. H. Dickinson. 1991. The ROLAI^{2}D lander: A benthic lander for the study of exchange across the sediment–water interface. Deep Sea Res. **38**: 505–529.

Schrag, D. P., G. Hampt, and D. W. Murray. 1996. Pore fluid constraints on the temperature and oxygen isotopic composition of the glacial ocean. Science **272**: 1930–1932. doi:10.1126/science.272.5270.1930

Subhas, A. V., N. E. Rollins, W. M. Berelson, S. Dong, J. Erez, and J. F. Adkins. 2015. A novel determination of calcite dissolution kinetics in seawater. Geochim. Cosmochim. Acta **170**: 51–68. doi:10.1016/j.gca.2015.08.011

Sulpis, O., C. Lix, A. Mucci, and B. P. Boudreau. 2017. Calcite dissolution kinetics at the sediment–water interface in natural seawater. Mar. Chem. **195**: 70–83. doi:10.1016/j.marchem.2017.06.005

Sulpis, O., B. P. Boudreau, A. Mucci, C. Jenkins, D. S. Trossman, B. K. Arbic, and R. M. Key. 2018. Current CaCO3 dissolution at the seafloor caused by anthropogenic CO_2. Proc. Natl. Acad. Sci. **115**: 11700–11705. doi:10.1073/PNAS.1804250115

Sun, X., J. Higgins, and A. V. Turchyn. 2016. Diffusive cation fluxes in deep-sea sediments and insight into the global geochemical cycles of calcium, magnesium, sodium and potassium. Mar. Geol. **373**: 64–77. doi:10.1016/j.margeo.2015.12.011

Wang, Z. A., X. Liu, R. H. Byrne, R. Wanninkhof, R. E. Bernstein, E. A. Kaltenbacher, and J. Patten. 2007. Simultaneous spectrophotometric flow-through measurements of pH, carbon dioxide fugacity, and total inorganic carbon in seawater. Anal. Chim. Acta **596**: 23–36. doi:10.1016/j.aca.2007.05.048

Acknowledgments

This work was supported by NSF Ocean Acidification (OCE-1834475). J.E.P.C. thanks the USC Wrigley Institute for Environmental Studies for PhD funding. H.A.B. thanks the Resnick Sustainability Institute for PhD funding. The authors would like to thank the editors, as well as David Burdige and an anonymous reviewer for their helpful questions and comments that improved the manuscript. The authors would like to sincerely thank Kalla Fleger for alkalinity and pH measurements on board; Matthew Quinan for dissolved silicate measurements; Rucha Wani and Emma Johnson for their contributions to the SIPR team at sea; and the science party, captain, and crew of the R/V Sally Ride SR2113 cruise. We also appreciate the discussions and laboratory support from Abby Lunstrum and assistance with silicate measurements from Doug Hammond. The authors also thank the Southern California Marine Institute and the captain and crew of the R/V Yellowfin for allowing us many SIPR test deployments.

Submitted 10 August 2022
Revised 11 November 2022
Accepted 06 December 2022

Associate editor: Clare E. Reimers